Blown Powder Laser Cladding with Novel Processing Parameters for Isotropic Material Properties

J. Liu[1], E. Fearon[1, 2], S.P. Edwardson[1], G. Dearden[1]

[1] Laser Engineering Group, Mechanical, Material & Aerospace Engineering, School of Engineering, the University of Liverpool, L69 3GH
[2] Systems and Products Development, Advanced Laser Technology Ltd, Manchester, M1 2NP

Abstract

A limitation for blown powder laser additive manufacturing in many applications is the material properties of parts made tend to show anisotropy due to directional solidification of the microstructure. Recent work reported here has identified novel low power processing conditions that yield equiaxed grain structures in 316L stainless steel and thus potentially eliminate material anisotropy. Initial observations show that the process window is affected by build height, substrate choice, powder, powder delivery rates, laser power and processing speed. A system has been developed to give precision layer height control via nozzle design and low powder delivery rates through an in-house design of powder hopper. Mechanical tests have been conducted under the novel processing parameters. Large amounts and uniform distribution of equiaxed structures compared to standard process conditions in 316L are found significantly. Moreover, cladding has been successfully produced with significantly low power around 350W, thus potentially improving process efficiency and set-up cost

1. Introduction

Additive manufacturing (AM) is receiving unprecedented attention from the mainstream media, the investment community, and national governments around the world. While there are multitude of laser based AM applications, laser cladding is the focus of this work. The Laser Cladding (LC) process can be known by many different names such as Laser Free Form Fabrication (LFFF), Direct Metal Deposition (DMD) or Directed Light Fabrication (DLF) (Mazumder, 2017).

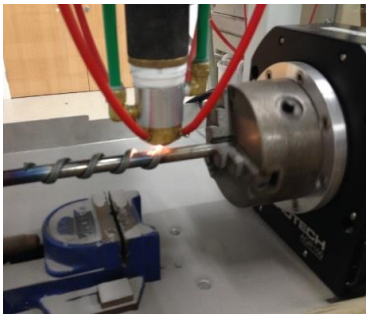

Figure 1: Apparatus of Laser Cladding at Liverpool with customised 4-port directional nozzles.

There are two main families of additive manufacturing technologies for production parts, powder bed technologies and blown powder technologies. Blown powder laser cladding (BPLC) is mainly explored in this work. In this process, metal powder is blown either coaxially or via a side feed into a laser generated melt pool, adding to its volume to form a fusion-bonded raised bead when cooled. This can then be built up layer by layer in a net shape process (Figure

1). This offers all the advantages of AM such as increased design freedom, light weight structures, new functionality and short production cycle times. In addition to powder bed technologies, BPLC also offers the addition of functionalities on existing parts with the same or a different material, compositional variation, repair of parts high value parts and no dimensional limits apart from machine size.

The application of LC also has advantages in aerofoil manufacturing with lower weight but high strength to weight ratio. This helps with shortening processing periods by around 80% as well as 20-50% reduction in cost (Ma, et al., 2013). Compared with conventional processing, laser cladding can provide high wear and corrosion resistance in terms of coating which is applied in the engine manufacture by Rolls-Royce and General Electric. In addition, rapid prototyping benefits from this technology.

A recent study on blown powder laser cladding by Song. et. al (Song, et al., 2016) has proved that addition of graded structures on existing part of different materials can clad. They applied Ni50Cr as blown powder cladding on 304 stainless steel successfully. In terms of different exploration purposes such as wear resistant, corrosion resistant and porosity, lots of materials have been used in BPLC like aluminides of titanium, nickel and iron in form of X3Al (Levin, et al., 2003). For experimental researches, numerical modelling will always be a good prediction for results since they are many factors affecting the cladding. Mazumder et. al (Mazumder, 2017) developed a self-consistent 3D transient model to examine the physical phenomena including heat transfer, melting/solidification phase change and liquid metal flow using a coaxial powder injection laser cladding process. The numerical results provided a good prediction to form a good metallurgical bonding by optimising the processing parameters. However, computational software and hardware still have limitations in simulating a model of accurate blown powder dynamics, melt pool morphology and melt pool fluid dynamic (Thompson, et al., 2015). Mechanical properties such as tensile, fatigue and impact testing are common applied to examine and evaluate the performance of the cladding structures. It's found that DLD parts gave similar or higher values of properties compared to wrong and cast materials (Shamsael, et al., 2015).

To better understand and investigate the BPLC process, high resolution microscopy of the generated metallurgies, micro-hardness test and tensile tests were completed as part of this work. Micro-hardness of laser cladding coupons varies significantly based on microstructural variations. Micro-hardness generally increases when microstructural variations decreases and keeps steady if majority of the structure is equiaxed when compared to the standard value for the material. Moreover, based on current novel low-power processing conditions, a majority equiaxed grain structure in stainless steel has been observed and thus potentially eliminating material anisotropy.

2. Experimental Work

2.1 Experimental Setup

A PRC 1.5kW CO_2 laser was used with a TEM^{01} mode shape. The laser is focused and delivered via a central nozzle mounted on the z-axis which is perpendicular to the cladding X-Y traverse table. This CNC table is controlled by the computer programmes which can build designed structures through G-code. The moving speed and layer height can be altered inside the CNC G-code as well as shape the component. The powder is fed into the four nozzles (in

red pipes, Figure 1) using a screw feed system on the top with Argon as assistant gas. The screw motor determines the powder mass. The gas flows for both powder feed and coaxial nozzles are controlled manually at a certain matching calibration to form an 'ideal' 'Y' shape of powder configuration (Figure 2 and Figure 3).

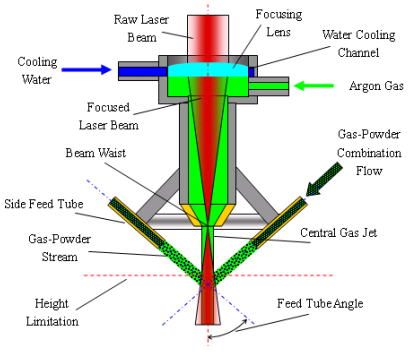

Figure 2: Schematic of Four-port powder feed nozzle at Liverpool.

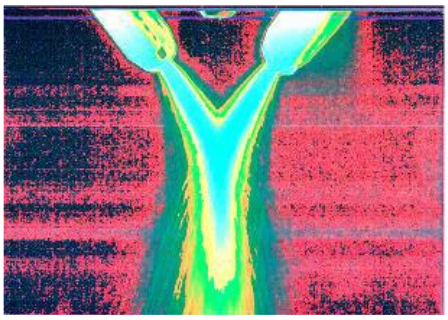

Figure 3: 'Y' shape of powder configuration.

Initial observations show that the process window is affected by build height, substrate choice, deposition material constraints or selection, powder delivery rates, laser power and process speed. Therefore, close control of process parameters is essential. The system has been specifically developed to give height control via this nozzle design and close control of very low powder delivery rate is possible with a custom design powder hopper. This nozzle can provide omnidirectional cladding with low angle powder feed and low velocity powder feed which helps to improve the catchment efficiency.

Apart from the effects from power, processing velocity and powder materials, layer height of cladding builds is another essential factor which affects the microstructures and related mechanism. In terms of geometrical accuracy, numerous researchers have designed many control methods to detect layer height and specific measurements. The benefit from this nozzle design at Liverpool is an open loop system that can utilize the shape of the powder stream to control the layer height which can be simply altered from the G-code programs. To investigate the effect of layer height, the height from 0.4mm to 1mm with 0.2mm segments were varied.

The powder material used in this work is 316L stainless steel powder with the composition listed in Table 1.

Table 1: Selected Austenitic Stainless Steel with chemical composition (nominal), wt. %.

Alloy	Fe	C	Cr	Ni	Mo	Si	Mn	S	P
316L	Balanced	0.03	16.0-18.0	10.0-14.0	2.0-3.0	1.0	2.0	0.03	0.045

Samples were sectioned, mounted and etched for analysis using optical microscope. To see the differences between single and multiple heating cycles of cladding builds, samples were selected from both intersected and non-intersected areas. Vickers hardness measurements were taken using a 500g load on the investigated surface. In terms of accuracy, five datum points were collected for each layer, equidistance throughout the sample. To explore the differences in mechanism between cladding and pure metal structures, a simple tensile test was taken.

Samples were sectioned, mounted and etched for analysis using optical microscope. To see the differences between single and multiple heating cycles of cladding builds, samples were selected from both intersected and non-intersected areas. Vickers hardness measurements were taken using a 500g load on the investigated surface. In terms of accuracy, five datum points were collected for each layer, equidistance throughout the sample. To explore the differences in mechanism between cladding and pure metal structures, a simple tensile test was taken.

2.2 Cladding Design and Processing

Two designed structures were laser clad and tested which both contained two intersecting circles of the same diameter. In terms of investigation on effect of multiple heating cycles and building methods, both intersected and non-intersected sections need to be taken into consideration when designing the geometries. Structure A (Figure 4 (a)) is intersected with a radius which built up with a linear method and laser indexing one layer by one layer. Structure B (Figure 5) two circles tangential which cladded in a helical manner (like infinity symbol '∞') and the laser was constantly indexing upwards.

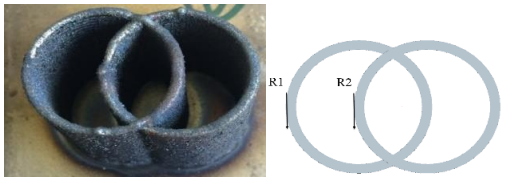

(a1) (a2)

Figure 4: (a1) Structure A with two circles intersected at half diameter; (a2) cladding path order.

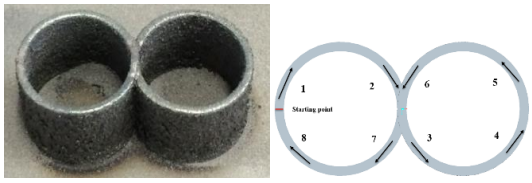

(b1) (b1)

Figure 5: (b1) Structure B with two circles intersected at the edge; (b2) cladding path order.

Both structures were laser clad under the same processing parameters which are shown in Table 2. All these parameters were kept constant during the cladding process. It is worth noting that the power used was only around 320W which was far less than the typical power of 800-1000W for similar processes.

Table 2: Consistent Processing Parameters of Structure A and B.

Power (W)	**Process Velocity (mm/s)**	**Powder Feed Rate (g/min)**	**Coaxial Gas Flow (L/min)**	**Powder Gas Flow (L/min)**
320	4	23	8	2.5

2.3 Cladding Design and Processing for Tensile Test

Another investigation into the mechanical property was achieved from tensile tests to obtain the ultimate tensile strength (UTS) and maximum load for the samples produced by laser cladding. To generate the tensile test coupons, the orientation of the deposited tracks in relation to the direction of the tensile force was designed in two directions, one was perpendicular to the tensile force (structure C) and the other parallel (structure D) shown in Figure 6.

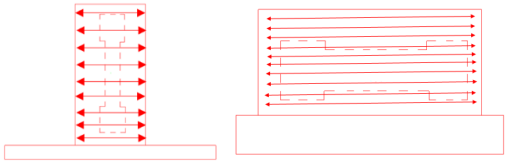

Figure 6: (c) Structure C with vertical cladding and (d) Structure D with horizontal builds used for tensile test (Davis, 2006).

Table 3 and Table 4 display the processing parameters and related dimensions for the two orientations. The parameters set were to explore the power effect and two types of powder catchment efficiency combined by power feed rate and gas flow rate. All coupons were laser clad with 1mm layer height under cladding speed of 4 mm/s.

Table 3: Processing parameters for structure C for vertical cladding tensile test samples and related dimensions (Figure 6 (c)).

Sample	Processing Parameters			Sample width (mm)	Sample thickness (mm)
	Power (W)	Powder feed rate (g/min)	Coaxial & powder gas flow (L/min)		
C1	320	23	8&2.5	29.92	1.38
C2	400	23	8&2.5	29.88	1.41
C3	600	23	8&2.5	30.61	1.46
C4	800	23	8&2.5	30.72	1.69

Table 4: Processing parameters for structure D with horizontal cladding tensile test samples and related dimensions (Figure 6 (d)).

Sample	Processing Parameters			Sample width (mm)	Sample thickness (mm)
	Power (W)	Powder feed rate (g/min)	Coaxial & powder gas flow (L/min)		
D1	320	23	8&2.5	29.21	1.38
D2	400	23	8&2.5	26.54	1.45
D3	600	23	8&2.5	25.97	1.83
D4	800	23	8&2.5	26.05	1.76

3. Results and Discussion

3.1 Microscopy Analysis

3.1.1 Structure A-- two circles intersected at half diameter

In terms of the non-intersected area, a typical directional solidification and epitaxial growth was observed in majority of cladding samples as well as strong microstructural variations. Towards the outside of the sample the microstructure is fine cellular whereas towards the center the microstructure is a mixed columnar dendritic and relatively coarse cellular (Figure 7(b)). This will be due to the outside of the melt pool cooling at a faster rate than the center of the melt pool causing fine cells to form at the outer regions (Fu, et al., 2008). For the intersected part, due to the complex melting and re-melting process, in which multiple solidification fronts meet from cladding occurring in two separate directions, a complex microstructure is observed. This is comprised of several phases of columnar dendritic, epitaxial cells and fine equiaxed cells. From Figure 7 and Figure 8, the layer height of cladding is significant to the microstructures and its variations. Sample 4 (structure A) with 1 mm layer height provides most equiaxed structures but still suffers from different level of epitaxial growth from the solute bands. In addition to the variation based on the distance from the substrate, it is difficult to generate a general summary based on the observation from Figure 8. In addition, the directional solidifications percentage was reduced by increasing the layer height, which can be seen from Figure 7 and Figure 8, due to the cooling rate of the cladding track that was affected.

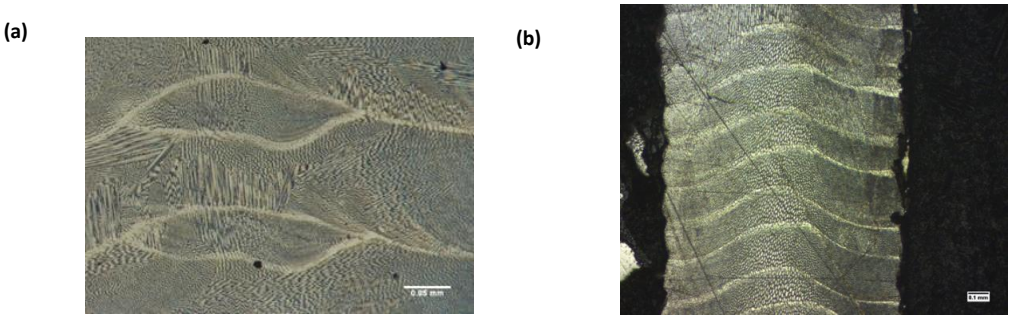

Figure 7: (a) Structure A with 0.4mm layer height intersected section, X100; (b) Structure A non-intersected section, X40.

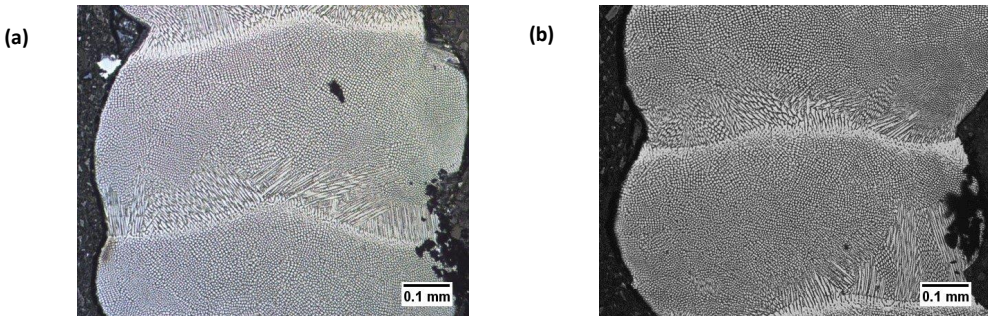

Figure 8: (a) Microstructure of Structure A non-intersection 8mm from substrate; (b) Microstructure of Structure A with 1mm layer height non-intersection 18mm from substrate, x100 magnification.

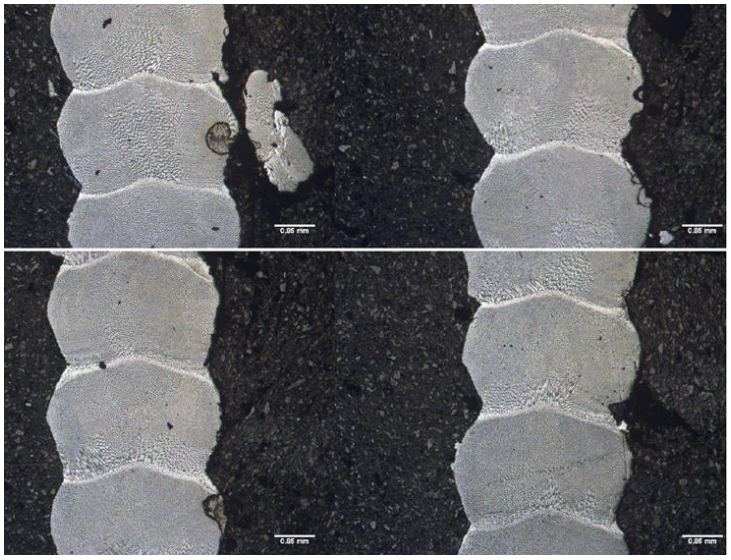

Figure 9: Overall view for the non-intersected region from the bottom to the top layers.

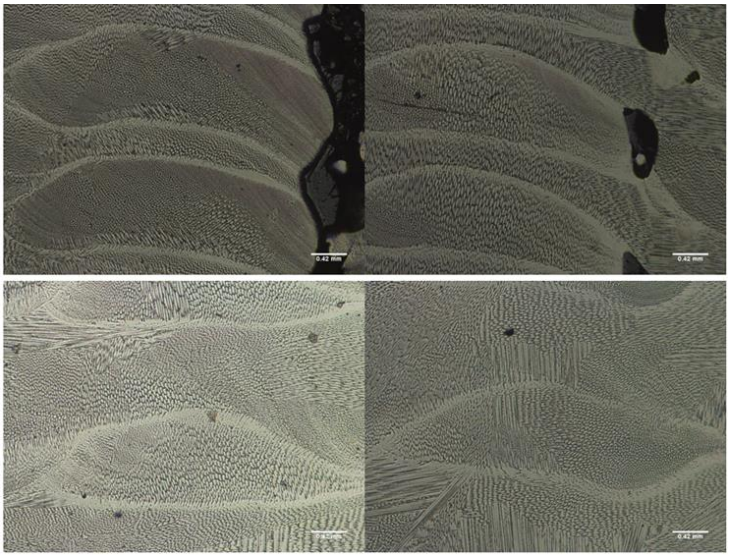

Figure 10: Overall view for the intersected region from the bottom to the top layers.

3.1.2 Structure B -- two circles intersected at the edge

Figure 11 (a-c) contains the typical characteristic microstructures of the laser cladding process. The solute banding from the solidification profile of the melt pool can be seen. The outside of the melt pool was cooling faster than the inside so that results in solidification directionality structures formed with epitaxial growth from the solute banding (Yue & Li, 2007). In other words, lots of dendritic structures propagating from solute bands in majority of layers of structure B. In the intersection part, majority of homogeneous cellular regions were concentrated with fewer variations in phases. Figure 11 (d) shows the equiaxed isotropic metallurgy observed under the low power conditions. This is a significant result for BPLC under this low power and related novel processing parameters. As equiaxed structures could eliminate material anisotropy.

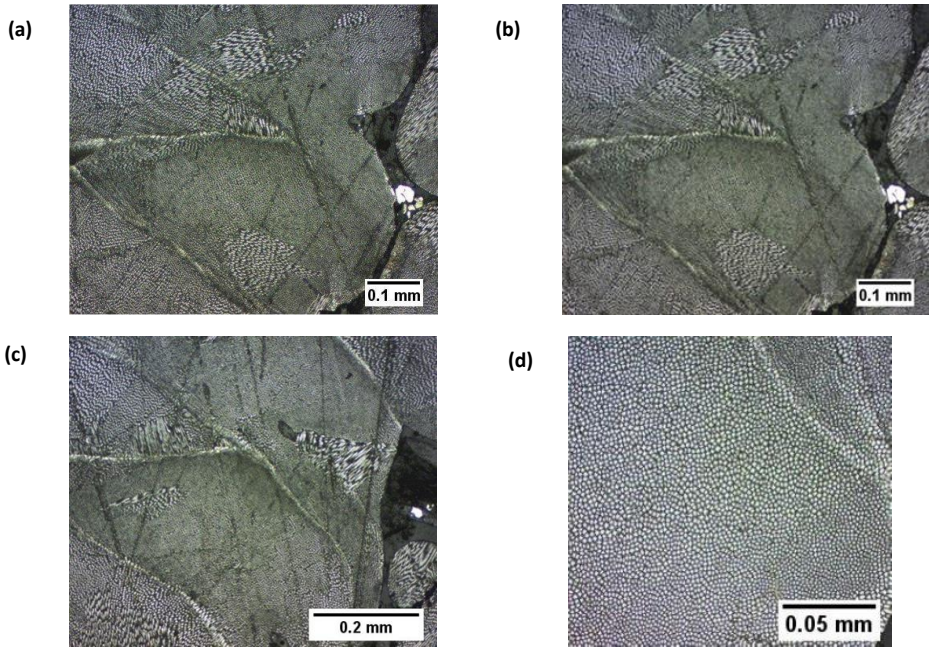

Figure 11: (a) (b) (c) Microstructure of Structure B with 1mm layer height intersection part on 6th, 9th, 12th layers from the substrate, with X40; (d) Microstructure of Structure B with 1mm layer height 11th layer intersected are zoom-in with X100 magnification.

The results of the microscopy investigation indicated that three kinds of structures were generated: dendritic cells, equiaxed cellular and solidification directionality microstructures (Kurz, et al., 2001). The distributions of them were varied along the distance from the substrate. Through altering the process parameters, homogeneous and equiaxed microstructures were found with uniform distribution and in large amounts under these novel processing conditions. The essential control factors involved layer height, the distance from the substrate and the intersected points. These have significant effects on various microstructural distribution and growth tendency due to the multiple heating cycles.

3.2 Micro-hardness Test

3.2.1 Structure A (Two circles intersected at half diameter)

As can be seen from Figure 12, the micro-hardness of structure A varied from 170-240HV. The points were taken from the midpoints of the solute bands at various distances from the substrate. Compared to the typical hardness of wrought AISI 316L stainless steel ranging from

170-220HV (Kurgan, et al., 2012), the results achieved were very close which may indicate hardening does not occur during the cladding process. However, a higher hardness value was expected or hardening should exist as fine cellular microstructures were found; high thermal gradients would result in high thermal stress which would cause the hardness increase of the microstructures. This discrepancy can be explained by the E/V values, as these were too low to cause the significant hardening effects in the material.

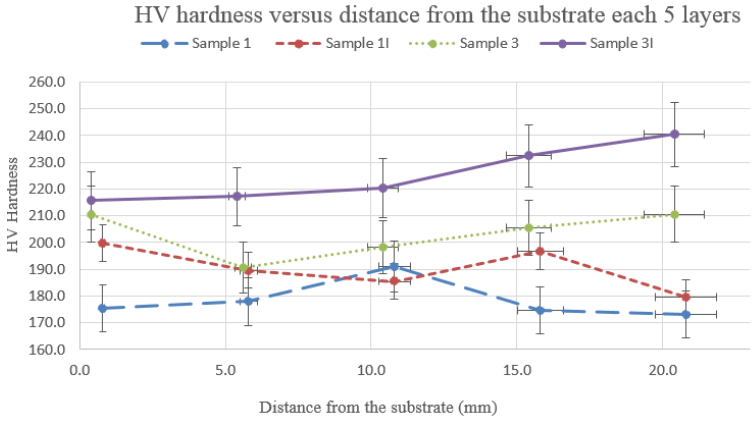

Figure 12: HV hardness of Structure A with 0.4mm layer height (sample 1) and 0.8mm layer height (sample 3) both intersected and non-intersected area (320W, 4mm/s cladding speed, powder feed rate 3000rpm, coaxial and powder gas flow are 8 and 2.5L/min).

Table 5: Micro-hardness and E/V value for Structure A both non-intersected and intersected area.

Sample	Average Vickers's Hardness (HV)	E/V (J/mm^3)
1 (Non-intersected, 0.4mm/layer)	189.5	159.18
1I (Intersected, 0.4mm/layer)	195.6	159.18
2 (Non-intersected, 0.6mm/layer	210.5	98.23
2I (Intersected, 0.6mm/layer)	220.3	98.23
3 (Non-intersected, 0.8mm/layer	207.6	71.31
3I (Intersected, 0.8mm/layer)	223.4	71.31
4 (Non-intersected, 1mm/layer	201.4	54.02
4I (Intersected, 1mm/layer)	215.6	54.02

3.2.2 Structure B ( )

The micro-hardness for the structure was ranging from 190HV to 250HV (Figure 13), these were higher than both structure A and the AISI standard. This indicates that the material

hardening occurred. This can be explained as a lower variation of microstructures and a smaller distribution of directionally solidification structures was observed. In addition, this indicated that the existence of equiaxed cellular structures would help to increase the hardness properties which concluded by Wu *et al* (Wu, et al., 2010).

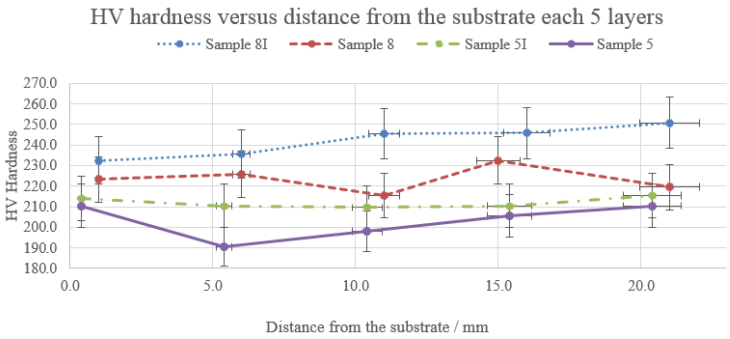

Figure 13: HV hardness of Structure B with 0.4mm layer height (sample 5) and 1mm layer height (sample 8) both intersected and non-intersected area (320W, 4mm/s cladding speed, powder feed rate 3000rpm, coaxial and powder gas flow are 8 and 2.5L/min).

Table 6: Micro-hardness and E/V value for Structure B both non-intersected and intersected area.

Sample	**Average Vickers's Hardness (HV)**	**E/V (J/mm^3)**
5 (Non-intersected, 0.4mm/layer)	205.5	162.07
5I (Intersected, 0.4mm/layer)	210.6	162.07
6 (Non-intersected, 0.6mm/layer)	210.5	101.58
6I (Intersected, 0.6mm/layer)	225.6	101.58
7 (Non-intersected, 0.8mm/layer)	211.3	73.67
7I (Intersected, 0.8mm/layer)	234.1	73.67
8 (Non-intersected, 1mm/layer)	242.1	56.15
8I (Intersected, 1mm/layer)	254.2	56.15

3.3 Tensile Test

The structures C and D (shown in Figure 6) were subjected to a tensile test. From the results generated in Table 7 and Table 8, it can be summarized that the horizontal samples which the track orientation was parallel to the tensile force show higher maximum breaking load and ultimate tensile stress than perpendicular ones.

Table 7: Averaged mechanical properties for vertical samples.

Sample	Max.Load (kN)	Ultimate Tensile Stress (MPa)	Elongation (%)
C1 (320W)	12.15	294.26	13.55
C2 (400W)	0.74	17.56	6.96
C3 (600W)	7.00	156.63	6.55
C4 (800W)	9.10	175.28	7.97

Table 8: Averaged mechanical properties for horizontal samples.

Sample	Max.Load (kN)	Ultimate Tensile Stress (MPa)	Elongation (%)
D1 (320W)	15.71	389.73	38.88
D2 (400W)	14.05	365.10	45.00
D3 (600W)	13.04	274.38	30.37
D4 (800W)	15.38	335.46	29.75

The cladding tracks perpendicular to the tensile force show a lower strength as the interfaces were weaker compared to the solid track area which means there are easier to be pulled apart from another track with weaker bonding (Dahotre, 1998). As discussed, directional solidification grains will grow from the solute band in different proportions based on changing processing parameters. In terms of microstructures under this condition, the directional solidification grains grew the same direction as the applied tensile force which allowed fewer barriers to dislocation movement; similar with being deformed or breaking easier and therefore a low mechanical strength. The failure mostly occurred from the track boundaries (Figure 14

(a)). For the sample with track direction along with the tensile force, higher strength and stiffness were achieved. The solute boundaries retained mechanical integrity and coherence during the pulling process. Moreover, the mobility of grains dislocations can determine the different degrees and direction of deformation. If a majority of equiaxed structures could be realized this would provide more barriers to prevent distortion and improve material anisotropy. From the final failure condition shown in Figure 14 (b), it can be seen that the failure path agreed with the solidification grains from different layers.

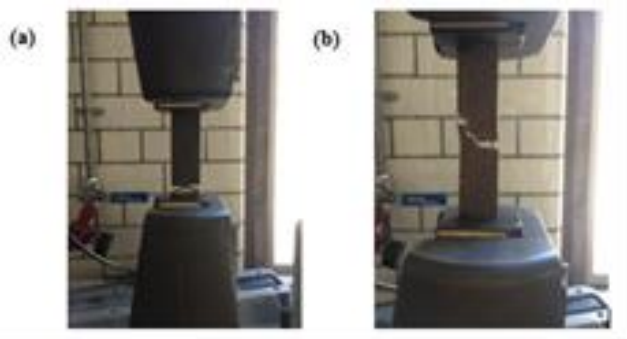

Figure 14: (a) Vertical build which tracks perpendicular to the tensile force; (b) horizontal build which tracks parallel to the force.

4. Conclusions

Based on the current work, it can be concluded that novel processing parameters have been found that provide better distributions of equiaxed structures. Due to the uniform distribution of homogeneous equiaxed structures, the structure B tested stronger in mechanical performance. In terms of tensile testing, structure D displayed a higher breaking load which related with cladding bonding efficiency and uniformity of microstructures. Processing powers of approximately 320W were used to generate these structures, this is significantly less than previous work in this area.

A limitation for laser-assisted blown powder deposition process in many applications is that the material properties of parts made tend to show anisotropy due to directional solidification of the microstructures as the re-melting conditions of the multi-layer process. This is not a problem for some applications such as an aero engine fan blade, but such anisotropy leads to severe design constraints in other AM components resulting in a requirement for post-process heat treatment. BPLC exploration in this work has identified novel processing conditions that yield equiaxed grain structures in stainless steel 316L and thus potentially eliminate material anisotropy. This is potentially a step change in the capability of AM.

Future work will confirm these findings in different materials and the variations of microstructures according to the distance from the substrate still need to be further explored. The process window is affected by build height, substrate choice, deposition material constraints or selection, powder delivery rates, laser power and process speed. Close control and optimisation of all these parameters will also form the basis for future work.

References

[1] Dahotre, N. B., 1998. Lasers for Metallic and Intermetallic Coatings. In: *Lasers in Surface Engineering.* Tullahoma: ASM International , p. 141.

[2] Davis, S. J., 2006. *Optimum Deposition Parameters for the Direct Laser Fabrication (DLF) of Quasi-Hollow Structures.* Manchester, Photon, Institute of Pgysics. .

[3] Fearon, E., 2004. *Optimisation of Layer Height Control in Direct Laser Deposition.* San Francisco, California, Laser Institute of America .

[4] Fu, J., Yang, Y., Guo, J. & Tong, W., 2008. Effect of cooling rate on solidification microstructures in AISI 304 stainless steel. *Materials Science and Technology ,* 24(Issue 8: Martensitic transformations), pp. 941-944.

[5] Kurgan, N., Sun, Y., Cicek, B. & Ahlatci, H., 2012. Production of 316L Stainless Steel Implant Materials by Powder Metallurgy and Investigation of their Wear Properties. *Materials Science,* 57(12), pp. 1876-1878.

[6] Kurz, W., Bezencon, C. & Gaumann, M., 2001. Columnar to Equiaxed Transition in Solidification Processing. *Science and Technology of Advanced Materials,* 2(1), pp. 185-191.

[7] Levin, A. A. et al., 2003. Phase Transformations after Long-time Annealing in Metastable Fe-Cr Alloy Films Prepared by Pulsed Laser Deposition. *Journal of Alloys and Compounds,* 360(1-2), pp. 107-117.

[8] Mahmood, K., Stevens, N. & Pinkerton, A. J., 2012. Laser surface modification using Inconel 617 machining swarf as coating material. *Journal of Materials Processing Technology,* Volume 212, pp. 1271-1280.

[9] Ma, M., Wang, Z., Wang, D. & Zeng, X., 2013. Control of shape and performance for direct laser fabrication of precision large-scale metal parts with 316L Stainless Steel. *Optics and Laser Technology,* Volume 45, pp. 209-216.

[10] Mazumder, J., 2017. Laser-aided direct metal deposition of metals and alloys. In: M. Brandt, ed. *Laser Additive Manufacturing.* Michigan: Woodhead Publishing, pp. 21-53.

[11] Shamsael, N., Yadollahi, A., Bian , L. & Thompson, S. M., 2015. An overview of Direct Laser Deposition for Additive Manufacturing; Part II: Mechanical Behavior, Process Parameter Optimization and Control. *Additive Manufacturing,* Volume 8, pp. 12-35.

[12] Song, B., Hussain, T. & Voisey, K. T., 2016. Laser Cladding of Ni50Cr: A Parametric and Dilution Study. *Physics Procedia,* pp. 706-715.

[13] Thompson, S. M., Bian, L., Shamsaei, N. & Yadollahi, A., 2015. An Overview of Direct Laser Deposition for Additive Manufacturing; Part I: Transport Phenomena, Modeling and Diagnostics. *Additive Manufacturing,* Volume 8, pp. 36-62.

[14] Wu, D., Liang, X., Li, Q. & Jiang, L., 2010. Laser Rapid Manufacturing of Stainless Steel 316L/Inconel718 Functionally Graded Materials: Microstructure Evolution and Mechanical Properties. *International Journal of Optics,* p. 5.

[15] Yue, T. M. & Li, T., 2007. Solidification Behaviour and the Evolution of Microstructure in the Laser Cladding of Aluminium on Magnesium Substrate. *Materials Transactions,* 48(5), pp. 1064-1069.